Ferroelectric surface chemistry: First-principles study of the $PbTiO_3$ surface

Kevin Garrity,[1,*] Arvin Kakekhani,[2] Alexie Kolpak,[3] and Sohrab Ismail-Beigi[2]
[1]*Department of Physics and Astronomy, Rutgers University, Piscataway, New Jersey 08854-8019, USA*
[2]*Department of Applied Physics and Department of Physics, Yale University, New Haven, Connecticut 06520-8120, USA*
[3]*Department of Materials Science and Engineering, Massachusetts Institute of Technology, Cambridge, Massachusetts 02139, USA*
(Received 14 April 2013; published 1 July 2013)

Ferroelectric surfaces provide a promising method for modifying surface reactions via an external electric field, which can potentially provide an avenue for tunable molecular binding and surface catalysis. Using first-principles density functional theory, we investigate how the properties of the $PbTiO_3$ surface vary with polarization and how these changes affect CO_2 and H_2O adsorption. We find that the polarized stoichiometric surfaces cancel the depolarizing field with an electronic reconstruction, which has a large effect on molecular binding energies. However, thermodynamically, the system will instead cancel the depolarizing field by adjusting the surface stoichiometry. Variation of the polarization and the environmental conditions can thus be used to systematically tune the surface chemistry over a wide range. In addition, we consider the addition of several different catalytic monolayers to the $PbTiO_3$ surface, and we find that additional surface layers can be used to modify the binding of molecules to the surface while still responding to the polarization of the substrate.

DOI: 10.1103/PhysRevB.88.045401 PACS number(s): 68.43.−h, 77.80.−e, 68.35.Md

I. INTRODUCTION

Due to a large, persistent response to electric fields, ferroelectric substrates offer a unique opportunity to tune the properties of a surface via an external field, potentially providing an avenue for advanced surface chemistry. By using an electric field to change the polarization direction of a ferroelectric substrate, one can potentially reversibly modify the surface Fermi level, atomic geometry, or even stoichiometry, all of which can alter the performance of the surface in applications.[1,2] This extra control over surface chemistry could potentially allow one to bind and release molecules from the surface or to turn reaction pathways on and off, enabling a new level of control over surface catalysis.[3,4]

Despite the promise of this approach, relatively little work has been done to understand the effects of polarization on the surface chemistry of ferroelectrics, and in particular on the binding of molecules to ferroelectric surfaces. Yun *et al.* performed a temperature programmed desorption (TPD) study of a variety of molecules on positively and negatively poled $LiNbO_3$ (0001) and found significant differences in desorption peak temperatures as well as pre-exponential factors.[5,6] In addition, Vohs *et al.* investigated small molecule adsorption on $LiNbO_3$, $BaTiO_3$, and lead-zirconate titanate and found that adsorption rates are affected by the substrate polarization, but adsorption energies are, instead, dominated by the concentration of defect sites on the surface.[7–10]

In complementary work, Wang *et al.* demonstrated that it is also possible to switch the polarization of thin film ferroelectrics by changing the oxygen environment in order to favor one surface over the other.[11] They grew 10-nm $PbTiO_3$ thin films and varied the oxygen pressure from 10^{-7} to 10^{1} Torr at temperatures between 550 and 950 K. By monitoring the lattice constant, they showed that low oxygen pressure results in an oxygen vacancy-related surface reconstruction that stabilizes a negative polarization, while the surface observed under high oxygen pressure favors a positively poled film.

Kolpak *et al.* used first-principles density functional theory to investigate the effect of polarization on the adsorption of molecules to a Pt layer supported by $PbTiO_3$.[2] They found that binding energies and geometries as well as molecular dissociation energies are affected by polarization and that these affects are strongest for a single monolayer of Pt covering the $PbTiO_3$ substrate. In addition, several experimental works on ferroelectric-supported metals, including $BaTiO_3$-supported Ni and $LiNbO_3$-supported Cu and Au, observed changes in catalytic activity correlated with the ferroelectric-paraelectric transition.[12–15]

In this work, we use first-principles density functional theory to investigate the effects of polarization on the (001) surface of $PbTiO_3$. We investigate the consequences of changing polarization on stoichiometric surfaces and determine the thermodynamically stable (nonstoichiometric) surface structures as a function of the film polarization. We then consider the adsorption of CO_2 and H_2O to both stoichiometric and nonstoichiometric surfaces.

We focus our efforts on surfaces that may improve CO_2 and H_2O catalysis because reactions involving these molecules are technologically important, especially to climate change. CO_2, which is produced by burning hydrocarbons, is a greenhouse gas, which may contribute to global warming, and finding a way to use or capture CO_2 is a major technological goal.[16,17] In addition, finding an efficient way to split H_2O into H_2 and O_2 would be a important step towards replacing hydrocarbons with H_2 in energy applications.[18]

Finally, in addition to looking at the $PbTiO_3$ surface itself, we also consider the effects of adding a single epitaxial surface layer of several different materials in order to combine the high polarization of $PbTiO_3$ with a material that has superior catalytic properties. Unfortunately, many of the transition metals commonly used as catalysts are not thermodynamically stable as monolayer films on $PbTiO_3$. However, we find several alkali earth metals and metallic oxides that are stable on $PbTiO_3$ and may have enhanced catalytic properties.

This paper is organized as follows. We briefly review the methods used in Sec. II, and apply them to stoichiometric and non-stoichiometric surfaces in Secs. III–IV. Epitaxial catalytic layers are discussed in Sec. V, and Sec. VI concludes the paper.

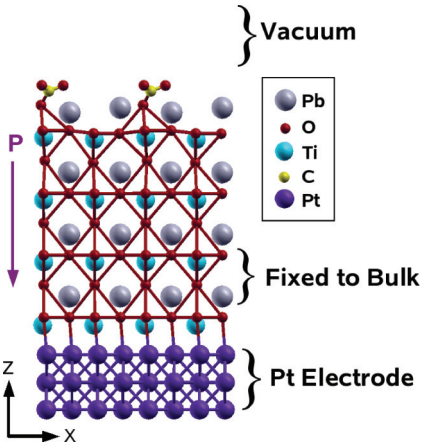

FIG. 1. (Color online) Schematic of simulation cell, shown for a negatively poled PbO-terminated surface with 0.5-ML CO_2. We use a slab geometry in the z direction, with vacuum above the surface and a Pt electrode on the opposite side of the $PbTiO_3$. The O−O bonds show octahedral cages around Ti.

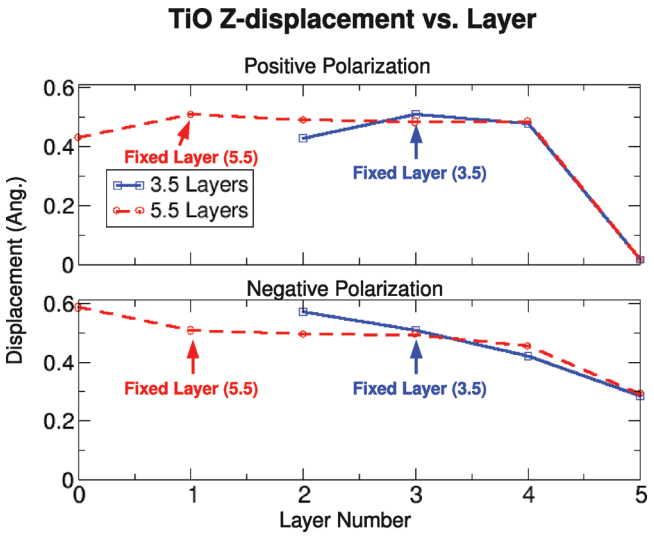

FIG. 2. (Color online) Average absolute value of Ti-O z-displacement in each layer for positively and negatively poled TiO_2-terminated surfaces. We compare slabs with 3.5 (blue squares, solid line) and 5.5 (red circles, dashed line) unit cells of $PbTiO_3$ and find similar surface geometry. The TiO_2 layers labeled layer 1 and layer 3 are fixed to bulk $PbTiO_3$ coordinates for the 5.5 and 3.5 layer slabs, respectively (the adjacent PbO layers to the left are also fixed).

II. METHODS

Our calculations are based on first-principles density functional theory calculations using a plane-wave basis set.[19,20] We use the PW91 GGA to approximate the exchange correlation function[21] and ultrasoft pseudopotentials to eliminate core electrons.[22,23]

We perform calculations in a slab geometry with the (001) surface of $PbTiO_3$ perpendicular to the z direction (see Fig. 11). We use a dipole correction to eliminate spurious electrostatic coupling between periodic copies in the z direction.[24] In order to simulate thick slabs of $PbTiO_3$, our unit cell consists of 3.5–4 unit cells of $PbTiO_3$, with three layers of Pt serving as a bottom electrode to provide an electron reservoir (see Fig. 1). We find that adding additional $PbTiO_3$ or Pt layers has no effect on CO_2 binding energies to within 0.01 eV.

We only consider polarization in the z direction, perpendicular to the surface. We fix our in-plane lattice constant to that of $SrTiO_3$, as that is known experimentally to fix the polarization to lie in the z direction.[25] In all cells, in order to simulate the polarization of a thick slab of $PbTiO_3$, but with reduced computational cost, we fix the second and third atomic planes (one PbO layer and one TiO_2 layer) from the bottom to their bulk values (the rest of the $PbTiO_3$ and Pt can relax). As can be seen in Fig. 2, this method reproduces the surface geometry of a slab of $PbTiO_3$, which has bulklike polarization in the center, despite the fact that a stoichiometric polarized slab with less than 10 unit cells of $PbTiO_3$ is higher energy than the equivalent paraelectric slab. While this method is suitable for simulating the surface properties of thick films, it precludes us from calculating the barrier for switching between a positive and negative polarization, as that calculation would require enough bulk material to stabilize a polarized film without constraints, which is beyond our computation capacity. Furthermore, the physical relevance of such a calculation is limited, as a real film will switch via complicated kinetic processes such as domain wall nucleation and motion and surface reconstruction, which are beyond the scope of this work.

When searching the phase space of atomic reconstructions, the possible reconstructions we consider are 0.5–2-ML adsorbed O and 0.5–1-ML O vacancies. In addition, for the PbO-terminated surface, we consider Pb vacancies, and for the TiO_2-terminated surface, we consider Ti vacancies. These calculations are all done in a $c(2 \times 2)$ surface unit cell, which allows for octahedral rotations and tilting. After using these initial calculations to get a rough idea of the phase space, we also considered larger unit cells and reconstructions for relevant surfaces (see, for example, the 4×1 reconstruction in Fig. 11). After determining the most stable surface for each polarization direction, we investigate CO_2 and H_2O binding sites by starting our relaxations with the molecules in several orientations (including disassociated) near each of the exposed atoms on the surface.

III. STOICHIOMETRIC SURFACES

We begin by examining the electronic structure of stoichiometric TiO_2-terminated $PbTiO_3$. For the paraelectric surface, we find that the surface states are similar to the bulklike region in the interior of the film, albeit with a reduced band gap due to the lower coordination number of surface atoms (see Fig. 3). In contrast, both the positively and the negatively poled surfaces undergo electronic reconstructions in order to cancel the depolarizing field arising from the polarization charge ($\sigma = \vec{P} \cdot \hat{z}$, see schematic in Fig. 4). For a stoichiometric surface, this is the only possible charge compensation mechanism (we consider atomic reconstructions in the following section).

On the positively poled surface, electrons move from the bottom electrode to the unoccupied d states on the surface Ti, which form the bottom of the conduction band [see Figs. 5(a) and 6]. This charge transfer screens the positive surface charge σ, and for a thick film will eliminate the depolarizing field

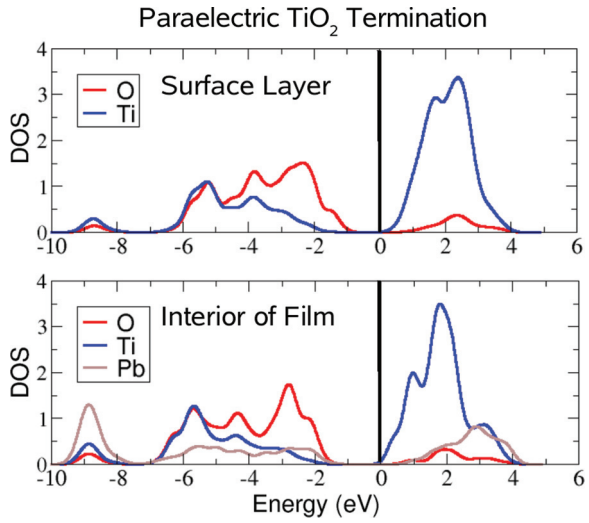

FIG. 3. (Color online) Projected density of states (DOS) for the TiO_2-terminated paraelectric surface. The energy is relative to the Fermi level. The top panel shows the DOS for the surface atoms, and the bottom panel shows DOS for bulk atoms.

across the $PbTiO_3$. The negatively poled surface has a similar electronic reconstruction; however, in this case, holes must move from the bottom electrode to the surface oxygen p states, which form the top of the valence band, in order to screen the negative surface charge [see Figs. 5(b) and 7]. This transfer of charges on both surfaces reduces the long-range depolarization field and stabilizes the ferroelectric distortion for thick films.

We note that the positively poled surface has a minor reconstruction, where half of the surface oxygen atoms are raised above the surface Ti, instead of below it as they would be in the bulk [see Fig. 5(a)]. This alternating of the

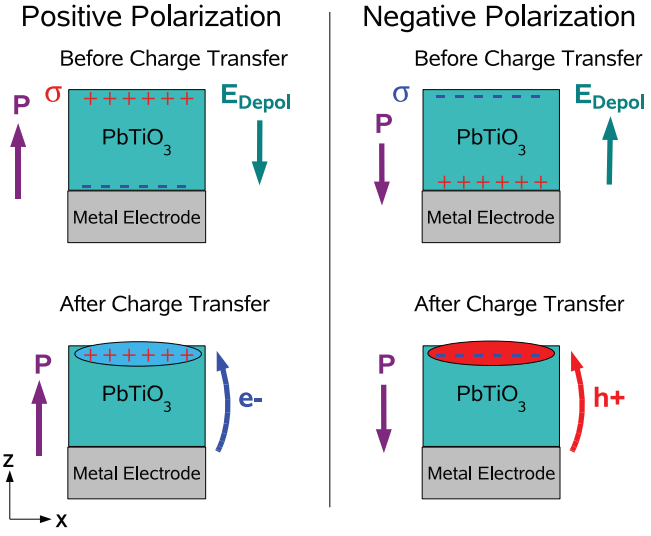

FIG. 4. (Color online) Schematic of electronic reconstructions. For both the positively poled (left) and negatively poled (right) surfaces, the polarization creates a surface charge σ, which results in a long-range depolarization field (E_{Depol}). In order to reduce this field, either electrons (positive surface) or holes (negative surface) transfer from the electrode to normally unoccupied surface states, modifying surface chemistry.

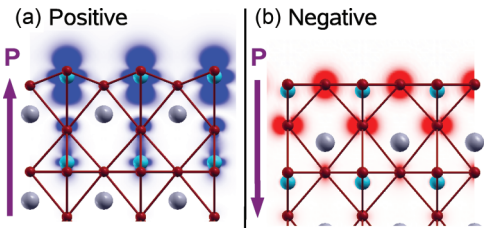

FIG. 5. (Color online) Integrated local density of states (DOS) for (a) positively poled and (b) negatively poled TiO_2-terminated surfaces. The positive surface (a) is integrated from the top of the conduction band to the Fermi level, and shows electrons in the Ti d orbitals on the surface. The negative surface (b) is integrated from the Fermi level to the top of the valence band, and shows holes in the p_{xy} orbitals on the surface O. Atomic colors are the same as Fig. 1.

surface O results in the surface layer having almost no net Ti-O displacement along the z direction, as the two types of surface O have large but opposite displacements in the z direction (see Fig. 2). However, this reconstruction is only 0.06 eV/1×1 surface unit cell lower in energy than a more bulklike configuration with both O below the surface Ti.

The polarization-induced electronic reconstruction has a large effect on both the CO_2 binding mode and binding energy (see Table I and Fig. 8). In the paraelectric case, the CO_2 forms a covalent bond with an O^{2-} on the surface, forming a carbonate $(CO_3)^{2-}$, as shown in Fig. 8(a). The electrons on the carbonate anion are localized between the carbon atom and a surface oxygen; additional interactions between the oxygen p states in the CO_2 and surface Ti also occur, as illustrated by the charge density plot in Fig. 8(e). This carbonate bonding geometry and covalent bond formation is a typical binding mode for CO_2 to an oxide surface,[26] in this case resulting in a moderate binding energy of 0.9 eV (see Table I). The negatively poled surface also forms a carbonate with a similar

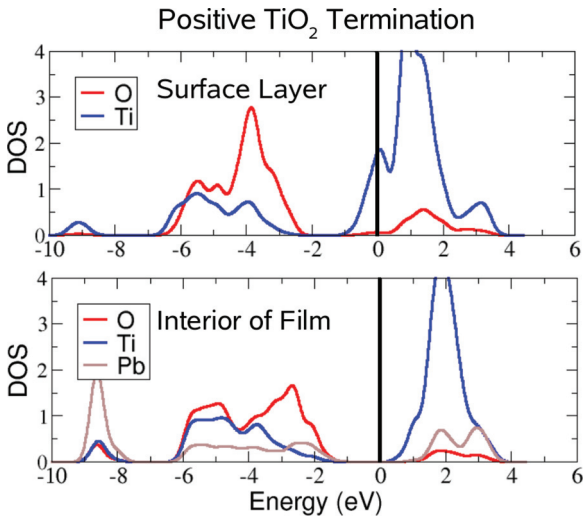

FIG. 6. (Color online) Projected density of states (DOS) for the TiO_2-terminated positively poled surface. The energy is relative to the Fermi level. The top panel shows the DOS for the surface atoms, and the bottom panel shows DOS for bulk atoms. Electrons screen the surface charge by moving into the Ti conduction band states, as seen in the top panel [see also Fig. 5(a)].

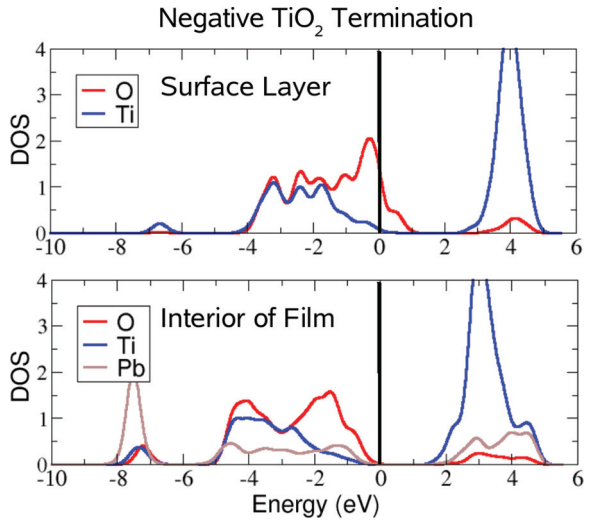

FIG. 7. (Color online) Projected density of states (DOS) for the TiO_2-terminated negatively poled surface. The energy is relative to the Fermi level. The top panel shows the DOS for the surface atoms, and the bottom panel shows DOS for bulk atoms. Holes screen the surface charge by moving into the O valence-band states, as seen in the top panel [see also Fig. 5(b)].

binding energy [see Figs. 8(b),8(e) and Table I]; although with a significant distortion of the surface Ti and O.

In contrast to the paraelectric and negatively poled cases, which form covalent bonds, the adsorption of CO_2 on a positively poled surface is primarily ionic, as illustrated in Fig. 8(c). This very strong bonding mode is primarily a charge transfer interaction driven by the screening electrons in the Ti conduction band states at the surface [see Fig. 5(a)]; these electrons transfer to normally empty antibonding states on the CO_2 (these states become lower in energy when the CO_2 bends[26]). The charge transfer can be observed in Fig. 8(f), which shows electrons leaving the red regions around the Ti and moving to the blue regions around the adsorbed molecule. In addition, this transfer of charge to the antibonding states of the CO_2 results in a very low dissociation energy for CO_2 on the positively poled surface [see Fig. 8(d)]. In fact, the binding of a dissociated O and CO is only 0.1 eV less stable than a CO_2 molecule (see Table I).

TABLE I. Binding energy of 0.5-ML CO_2 on stoichiometric $PbTiO_3$ surfaces (see Fig. 8).

Termination	Polarization	Geometry	Binding energy (eV)
TiO_2	Paraelectric	Carbonate $(CO_3)^{2-}$	0.9
TiO_2	Negative	Carbonate $(CO_3)^{2-}$	1.2
TiO_2	Positive	$(CO_2)^{2-}$	2.0
TiO_2	Positive	Dissociated CO and $(O)^{2-}$	1.9
PbO	Paraelectric	Carbonate $(CO_3)^{2-}$	0.5
PbO	Negative	Carbonate $(CO_3)^{2-}$	0.9
PbO	Positive	$(CO_2)^{2-}$	0.2

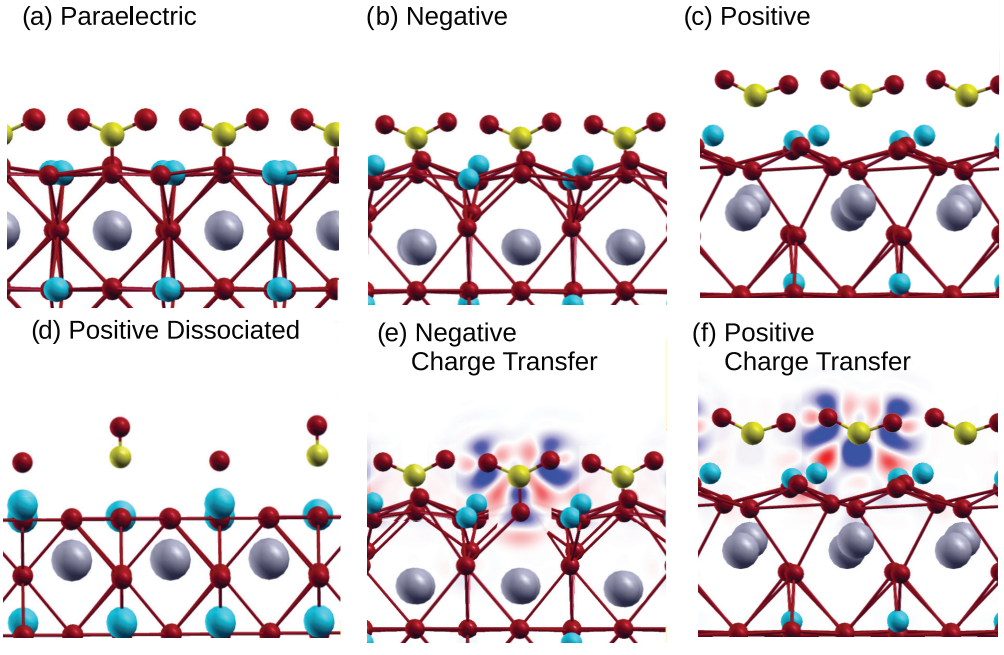

FIG. 8. (Color online) (a)–(c) Low-energy binding geometry for 0.5-ML CO_2 on a stoichiometric TiO_2-terminated surface for (a) paraelectric, (b) negative, and (c) positive polarizations. (d) Metastable dissociated geometry on positively poled surface (see Table I). (e)–(f) Smoothed electron transfer plots for the surfaces in (b) and (c). The background colors show how the electrons rearrange when the CO_2 and the surface are allowed to interact, i.e., the difference in electron density between the full calculation of the molecule plus the surface and separate calculations of the molecule and surface but with all atomic atomic positions fixed to those from the full calculation, including surface and molecule. The positive surface (f) shows a net transfer of electrons from surface Ti to the dissociated CO and O, while the negative surface (e) shows covalent bond formation.

These calculations suggest that a switchable stoichiometric TiO_2-terminated $PbTiO_3$ surface would be very useful for CO_2 catalysis. First, the positively poled surface could be used to bind and greatly lower the dissociation energy of a CO_2 molecule, allowing a reaction to proceed. Then, the polarization could be flipped, and the negatively poled surface would release the products. However, this strong binding of the CO_2 to the positively poled surface is partially due to the unstable state the surface is in prior to the interaction with the molecule. Instead, it is likely that the bare surface itself will reconstruct in order to reduce the number of electrons in the conduction band, possibly interfering with this promising result.[27] We investigate the effect of such atomic reconstructions next.

IV. NONSTOICHIOMETRIC SURFACES

A. Surface thermodynamics

In order to compare the relative thermodynamic stabilities of nonstoichiometric $PbTiO_3$ surfaces, we compare the zero-temperature and zero-pressure surface free energy per area,

$$F_{\text{surf}}(\mu_{\text{Pb}},\mu_{\text{Ti}},\mu_{\text{O}}) = E_{\text{Tot}} - N_{\text{Pb}}\mu_{\text{Pb}} - N_{\text{Ti}}\mu_{\text{Ti}} - N_{\text{O}}\mu_{\text{O}}, \quad (1)$$

where E_{Tot} is the total energy of the surface per unit area, N_i is the number of atoms of species i, and μ_i is the chemical potential of species i (the possible species are Pb, Ti, and O). The chemical potential of a species is the energy required to take an atom of that type from a thermodynamic reservoir and add it to the surface.

As discussed in Ref. 28, by using the energy to approximate the Gibbs free energy, we are neglecting both the effects of pressure and vibrations on the free energy. For solids, the contribution of pressure to the Gibbs free energy is negligible for pressures considered in this work.[28] While the role of vibrational free energy is larger, calculations of the difference in vibrational free energy due to changes in adatom binding sites are typically on the order of 50 meV/atom at 600 K, which is not enough to change any conclusion in this work.[29]

When calculating the surface free energy, we assume that bulk $PbTiO_3$ is stable in our system; therefore the relevant region of phase space is that in which $PbTiO_3$ is stable with respect to the formation of compounds like PbO or TiO_2 (see Table II). We use DFT to calculate the formation energy of these bulk compounds. Our first requirement is that bulk $PbTiO_3$ be in equilibrium with our reservoirs, which means adding or subtracting a full unit cell of $PbTiO_3$ from our system does not change its free energy. This creates the constraint that

$$E_{\text{PbTiO}_3} = \mu_{\text{Pb}} + \mu_{\text{Ti}} + 3\mu_{\text{O}}, \quad (2)$$

which allows us to eliminate μ_{Ti} and only consider the two-dimensional phase space $(\mu_{\text{O}},\mu_{\text{Pb}})$. In addition, we require that our surfaces are stable with respect to the formation of bulk Pb, Ti, TiO_2, and PbO, which adds the following constraints:

$$\mu_{\text{Pb}} \leqslant E_{\text{Pb}}, \quad (3)$$

$$\mu_{\text{Ti}} = E_{\text{PbTiO}_3} - \mu_{\text{Pb}} - 3\mu_{\text{O}} \leqslant E_{\text{Ti}}, \quad (4)$$

$$\mu_{\text{Pb}} + \mu_{\text{O}} \leqslant E_{\text{PbO}}, \quad (5)$$

$$\mu_{\text{Ti}} + 2\mu_{\text{O}} = E_{\text{PbTiO}_3} - \mu_{\text{Pb}} - \mu_{\text{O}} \leqslant E_{\text{TiO}_2}. \quad (6)$$

TABLE II. DFT formation energies and experimental $\Delta_f H^0$ of various compounds. DFT formation energies are relative to bulk crystals at zero temperature for all elements except O, which is relative to an isolated atomic O_2 molecule. We also include the atomization energy of O_2, which is the energy required to split an O_2 molecule into two O atoms.

Compound	DFT formation energy (eV)	Experimental $\Delta_f H^0$
PbO	−2.59	−2.27 [30]
TiO_2	−9.85	−9.73 [30]
$PbTiO_3$	−12.77	−12.42 [31]
SrO	−5.87	−6.14 [30]
RuO_2	−2.85	
Rb_2O	−3.09	
O_2	6.64	5.23 [32]

In addition to the above limits, we require that the oxygen chemical potential corresponds to a gas with a temperature and pressure that is achievable under typical experimental conditions. This places the additional limit that

$$\mu_{\text{O}} \leqslant \tfrac{1}{2}E_{\text{O}_2}. \quad (7)$$

Any thermodynamically stable surface must have the lowest free energy at a given set of $(\mu_{\text{O}},\mu_{\text{Pb}})$ that is allowed by the above constraints. The allowed region of phase space corresponds to the area inside the red lines in the phase diagrams shown in Figs. 9, 10, and 12. In order to improve comparison with experiment, we also apply a correction to the formation energy of an O_2 molecule from two O atoms, which is well known to be overestimated in GGA, and also sensitive to the details of the pseudopotential used in the calculation.[33,34] While the O_2 molecule itself is not a focus of this work, this error shifts the zero of the calculated oxygen chemical potential, reducing agreement with experimental oxygen chemical potentials. We correct for this by referencing μ_{O} to the energy of atomic oxygen in DFT plus one-half of the experimental formation energy of O_2 (rather than the bare DFT formation energy).[35] This correction has no effect on

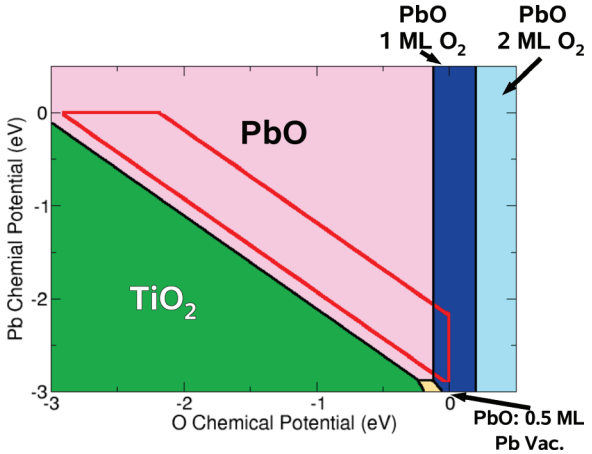

FIG. 9. (Color online) Phase diagram of the paraelectric surface as a function of μ_{O} and μ_{Pb}. Each colored region is the thermodynamically stable structure for those chemical potentials. The physically allowed region is inside the red lines. The only stable structure in the majority of phase space is the stoichiometric PbO termination.

the relative stability of structures in DFT, but improves the comparison with experimental phase diagrams.

B. Bare surfaces

We use the methods in Sec. IV A to find the most stable stoichiometry and geometry of the surface throughout the range of chemical potentials in which $PbTiO_3$ is stable. In agreement with previous work,[36] we find that the surface is always PbO-terminated; however, by expanding our phase space to include atomic reconstructions, we find that the stoichiometry of the top-most PbO layer changes in response to the polarization in order to compensate the surface charge and eliminate the depolarization field.

We begin by looking at the paraelectric surface. Figure 9 shows that except for regions of very high oxygen chemical potential, which causes O_2 molecules adsorb to the surface, the paraelectric surface is terminated by a stoichiometric charge neutral PbO layer, as expected for a system with no polarization-induced surface charge. We find that the system does have a $c(2 \times 2)$ reconstruction due to TiO_6 octahedral rotations in the second atomic layer, consistent with experiment.[37]

The situation is very different for the polarized surfaces, as neither polarized surface is terminated by a stoichiometric PbO layer for any set of chemical potentials. For the negatively poled surface, this can be seen in Fig. 10, which shows that neither stoichiometric termination is ever the lowest energy structure at any combination of Pb and O chemical potentials. Instead of forming a stoichiometric termination, which requires an electronic reconstruction to cancel the depolarizing field [see Sec. II and Figs. 4, 5(b), and 7], the system undergoes an atomic reconstruction. Specifically, over a wide range of μ_O, the system forms oxygen vacancies on the surface. These oxygen vacancies act as positively charged defects that serve to cancel the depolarizing field through the substrate in the same way that the stoichiometric negatively poled surface accumulates holes. Equivalently, the oxygen

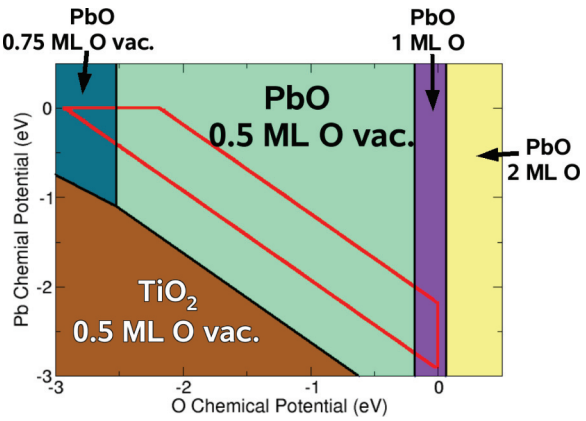

FIG. 10. (Color online) Phase diagram of a negatively poled surface as a function of μ_O and μ_{Pb}. Each colored region is the thermodynamically stable structure for those chemical potentials. The physically allowed region is inside the red lines. Stable structures are all PbO terminated, and have 0.75-ML O vacancies, 0.5-ML O vacancies (see Fig. 11), and 1.0-ML adsorbed O (at very high μ_O).

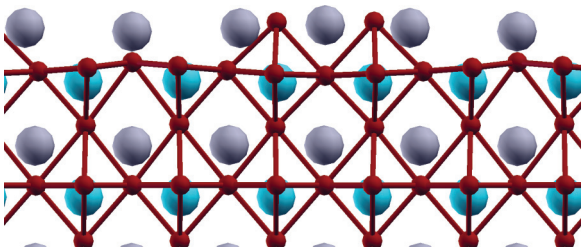

FIG. 11. (Color online) Atomic structure of a negatively poled PbO-terminated surface with 0.5-ML vacancies arranged into a 4×1 reconstruction. This structure corresponds to the green region in the center of Fig. 10.

vacancies can be viewed as electron donors, with the donated electrons filling in the holes caused by the depolarization field.

Over most of the relevant range of chemical potentials, the negatively poled surface has 0.5-ML oxygen vacancies (see the large light green region in the center of Fig. 10). Of the structures we have tried, which are 2×1, $c(2 \times 2)$, 4×1, $c(4 \times 2)$, and 2×2, the lowest energy configuration is for the vacancies to arrange themselves into a 4×1 pattern as shown in Fig. 11. This pattern allows the three Pb^{2+} with surface O neighbors to break symmetry and decrease their distance from two of the O by 0.4–0.5 Å. Also, the surface Pb with no surface O neighbors moves towards the bulk, decreasing its distance to its second layer O neighbors by 0.2 Å. Relative to the $c(2 \times 2)$ reconstruction, where each Pb also breaks symmetry, but only has one close O neighbor, this reconstruction is 0.2 eV/u.c. more stable. The reconstruction is consistent with the experimental observation of a 4×1 reconstruction on the negatively poled surface.[11]

The positively poled surface is similar to the negatively poled surface in that the stoichiometric surface is never thermodynamically stable (see Fig. 12). This surface, which prior to reconstruction would have extra electrons in the conduction band [see Figs. 4, 5(a) and 6], reconstructs to have either extra O adsorbed on the surface (high μ_O, high μ_{Pb}), or Pb vacancies

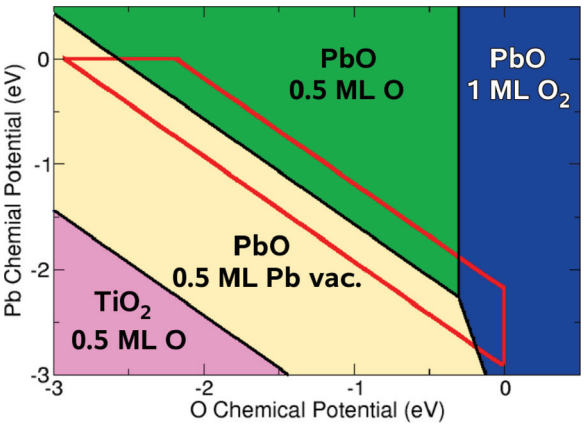

FIG. 12. (Color online) Phase diagram of the positively poled surface as a function of μ_O and μ_{Pb}. Each colored region is the thermodynamically stable structure for those chemical potentials. The physically allowed region is inside the red lines. Stable structures are all PbO terminated, and have 0.5-ML adsorbed O [see Figs. 13(a) and 13(b)], 0.5-ML Pb vacancies [see Fig. 13(c)], and 1 ML adsorbed O_2 (at very high μ_O).

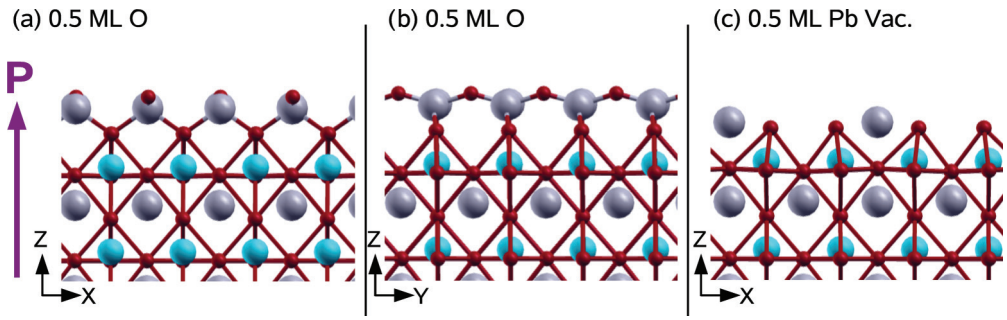

FIG. 13. (Color online) Selected thermodynamically stable structures for the positively poled surface. (a) and (b) are two views of the PbO surface with 0.5-ML adsorbed oxygen, which corresponds to the dark green triangular region in the upper part of Fig. 12. The Pb atoms have left their bulk positions and moved half a unit cell in the y direction, which results in an shorter Pb-O distance, which is closer to bulk PbO. The adsorbed O is between two Pb. (c) The PbO surface with 0.5-ML Pb vacancies, which corresponds to the orange region in Fig. 12.

(low μ_O, low μ_{Pb}) (see Fig. 13). The extra O atoms act as electron acceptors and the Pb vacancies act as hole donors, both of which reduce the number of electrons in the conduction band while still compensating the depolarization field. The surface with extra oxygen [see Figs. 13(a) and 13(b)] has an interesting reconstruction, where each Pb atom moves 0.5 unit cell in the y direction, which reduces its distance to the surface O while maintaining a large displacement in the z direction.

C. CO_2 binding

Armed with knowledge of how polarization affects surface geometry and stoichiometry, we investigate the effect of these changes on surface chemistry and reactivity. Specifically, we will again look at CO_2 binding to the surface. We consider the binding of CO_2 to the four surfaces that are stable in large regions of phase space. The results are summarized in Table III.

Allowing atomic reconstructions generally reduces the largest CO_2 binding energies (compare Tables I and III). In particular, the very large binding energy associated with the charge transfer binding mode of the positively poled TiO_2-terminated surface does not occur on either of the thermodynamically stable positively poled surfaces. On the stoichiometric surface, this binding mechanism is driven by the electrons in high-energy Ti d states, and because the atomic reconstructions eliminate these high-energy electrons, the related binding mode is also suppressed.

While most of the surfaces demonstrate the typical carbonate binding geometry, with the CO_2 forming a covalent bond with one of the exposed oxygen atoms (see Fig. 14), there is still significant variation in the binding energy with polarization. In particular, the positively poled surface demonstrates the importance of atomic geometry and stoichiometry to molecular binding. The positively poled surface with adsorbed oxygen, which occurs for surfaces with high μ_O and high μ_{Pb} [see Figs. 12, 13(a), and 13(b)], has no chemisorption mode for CO_2 binding because the unusual positions of the surface Pb and adsorbed oxygen prevent carbonate formation. On the other hand, the positively poled surface with Pb vacancies has enough room for the CO_2 to displace a surface Pb atom and reach a stable binding site [compare Figs. 14(a) and 14(b)].

Table III suggests the possibility of using thermodynamically stable $PbTiO_3$ surfaces to bind and release CO_2 by switching the polarization. In particular, in the part of the phase diagram with high μ_O and high μ_{Pb}, switching the polarization will cycle between the negatively poled surface with 0.5-ML oxygen vacancies, which forms a covalent bond with CO_2 [see Fig. 14(c)], and the positively poled surface with 0.5-ML added oxygen, which binds CO_2 only via weaker physisorption [see Fig. 14(a)]. However, while these differences in binding with polarization are interesting as a proof of principle, the low total magnitude of the binding limits potential applications. In particular, attempting to use this surface to bind and release CO_2 will require sensitive control of temperatures around 180 K.[38] Therefore, in Sec. V, we consider other materials in the hope of finding a larger effect.

D. H_2O binding

In addition to CO_2 binding, we also consider the binding of gas phase H_2O molecules to the thermodynamically stable $PbTiO_3$ surfaces. Like CO_2, both the binding energy and binding mode of H_2O depend on the polarization direction and oxygen coverage. The results are summarized in Table IV.

The paraelectric PbO-terminated surface has two competitive H_2O binding modes. The most favorable binding mode for this surface has an H_2O molecule forming a hydrogen bond

TABLE III. Binding energy of 0.5-ML CO_2 to thermodynamically stable surfaces.

Polarization	Termination	Stoichiometry (ML)	Binding geometry	Figure	Binding energy (eV)
Positive	PbO	+0.5 O	Physi.	14(a)	0.13
Positive	PbO	−0.5 Pb	$(CO_3)^{2-}$	14(b)	0.66
Negative	PbO	−0.5 O	$(CO_3)^{2-}$	14(c)	0.50
Paraelectric	PbO	0	$(CO_3)^{2-}$	14(d)	0.29

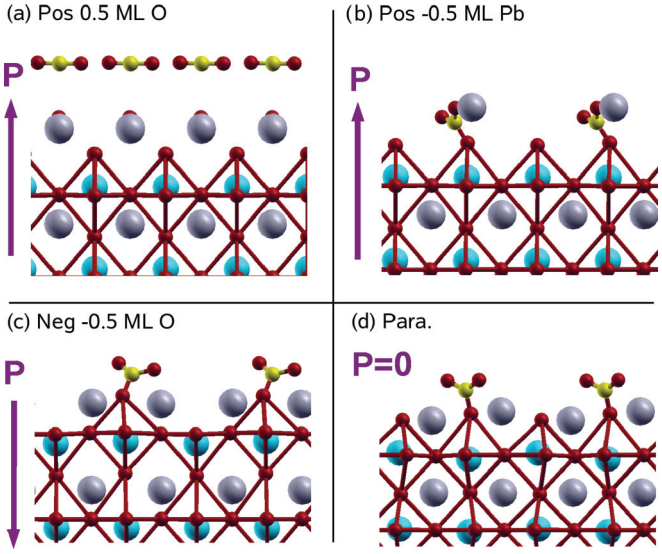

FIG. 14. (Color online) Binding of 0.5-ML CO_2 to selected thermodynamically stable surfaces (see Table III). (a) Physisorption to a positively poled surface with 0.5-ML O. (b) Carbonate bonding to a positively poled surface with 0.5-ML Pb vacancies. (c) Carbonate bonding to a negatively poled surface with 0.5-ML oxygen vacancies. (d) Carbonate bonding to a stoichiometric PbO-terminated paraelectric surface.

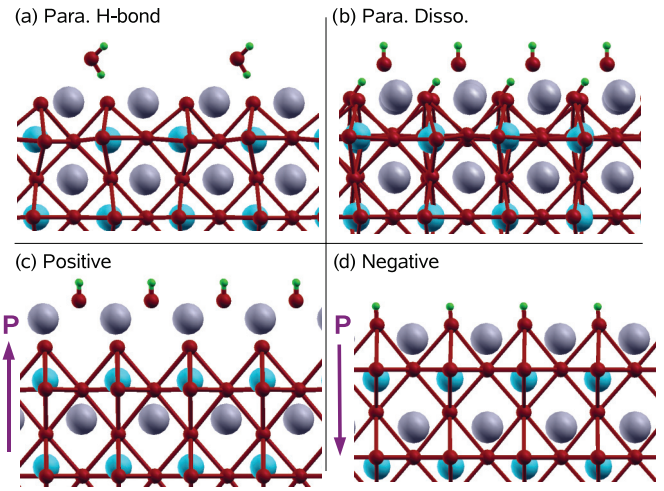

FIG. 15. (Color online) Binding of 0.5-ML H_2O to selected thermodynamically stable surfaces (see Table IV). H is in green (other colors the same as Fig. 1). (a) Hydrogen bonding to a paraelectric surface. (b) Disassociated bonding to a paraelectric surface. (c) Disassociated bonding to a positively poled surface with 0.5-ML adsorbed oxygen. (d) Disassociated bonding to a negatively poled surface with 0.5-ML oxygen vacancies.

to a surface oxygen atom, with a binding energy of 0.76 eV [see Fig. 15(a)]. The H-O bond length for the hydrogen bond is 1.6 Å, as opposed to a covalent bond distance of 1.0 Å. The other binding mode, which is 0.20 eV less stable, again has two covalent H-O bonds plus a hydrogen bond; however, in this case, the H_2O dissociates and the H atom binds covalently to a surface oxygen [see Fig. 15(b)].

In contrast to the paraelectric surface, the thermodynamically stable negatively poled surface with 0.5-ML oxygen vacancies shows a strong preference for the dissociated binding geometry [see Fig. 15(d) and Table IV]. Like the dissociated binding mode on the paraelectric surface, the dissociated H again bonds to a surface O, forming an OH. However, instead of forming a hydrogen bond with the surface, the remaining OH fills in the oxygen vacancy site. The end result is the same as a stoichiometric PbO-terminated surface with an additional 1 ML atomic H bonded to the surface oxygen. The change from $O^{2-} + H_2O \rightarrow 2\,(OH)^-$ results in a strong binding energy of 1.14 eV.

Interestingly, the low-energy binding mode of H_2O to the thermodynamically stable positively poled surface with 0.5 ML adsorbed O is very similar to the binding mode of the negatively poled surface [see Fig. 15(c)]. Again, the H_2O dissociates, and the H bonds to the extra surface O atom. The $(OH)^-$ then fills in the empty O adsorption site, between two Pb atoms, resulting in a surface with a 1×1 reconstruction and 1 ML adsorbed $(OH)^-$. Much like the negatively poled surface, the end result is $O^{2-} + H_2O \rightarrow 2\,(OH)^-$, which results in a more stable system and a binding energy of 0.76 eV. The difference between the two polarizations is that the negatively poled surface has 1 ML less oxygen than the positively poled surface, due to the differing surface charges.

These surfaces are potentially useful because they show that (a) one can dissociate H_2O into OH by switching between a paraelectric surface and either polarized surface, and (b) one can change the binding energy of the dissociated H_2O by flipping the polarization; however, more work must be done in order to understand how these changes will affect practical catalytic reactions.

V. EPITAXIAL CATALYTIC LAYERS ON $PbTiO_3$

While our results for CO_2 adsorption on $PbTiO_3$ are very interesting as a proof of principle, we attempt to improve the surface's catalytic properties. In particular, we would like a surface that (a) is thermodynamically stable, (b) has strong

TABLE IV. Binding energy of 0.5-ML H_2O to several surfaces using both a disassociated geometry and a hydrogen-bonded geometry. The top three surfaces are thermodynamically stable, the bottom two are included for comparison.

Polarization	Termination	Stoichiometry (ML)	Dissociated binding (eV)	H-bond binding (eV)	Figure
Paraelectric	PbO	0	0.56	0.76	15(a) and 15(b)
Positive	PbO	+0.5 O	0.76	0.49	15(c)
Negative	PbO	−0.5 O	1.14	0.20	15(d)
Positive	PbO	0	0.04	0.18	
Negative	PbO	0	1.05	0.64	

TABLE V. Binding energy of atomic O and CO_2 to various stoichiometric surfaces. Oxygen will compete with CO_2 for binding sites, which for realistic oxygen chemical potentials will cause many of the surfaces to be covered in excess oxygen, preventing the binding of CO_2.

Termination	Monolayer	Polarization	0.5-ML O binding (eV/2×1)	1.0-ML O binding (eV/2×1)	CO_2 binding (eV/2×1)	Figure
TiO_2	$SrRuO_3$	Positive	1.5	3.2	0.6	17(a)
TiO_2	$SrRuO_3$	Negative	0.1	1.2	0.7	
TiO_2	$SrRuO_3$	Paraelectric	1.3	2.1	0.7	
TiO_2	SrO	Positive	3.4	4.2	1.3	
TiO_2	SrO	Negative	1.1		1.6	
TiO_2	SrO	Paraelectric	0.8	0.8	1.5	17(b)
TiO_2	Rb	Positive	5.8	10.2	2.3	
TiO_2	Rb	Negative	1.4	2.9	1.4	17(c)
TiO_2	Rb	Paraelectric		2.0	1.8	

CO_2 binding for at least one polarization, and (c) shows a large change in binding energy with polarization. Preferably, this material will be metallic, so that the Fermi level on the surface can change with polarization, altering the binding energy without changing the stoichiometry of the surface.

Most of the typical transition metals used for catalytic applications are not thermodynamically stable on a $PbTiO_3$ surface. These transition metals have large cohesive energies, and prefer to aggregate into bulklike clusters on the surface. For instance, on the TiO_2-terminated surface, a monolayer of Pt is unstable with respect to the formation of bulk Pt by 0.6 eV/Pt for the positively poled surface and 1.2 eV/Pt for a negatively poled surface. We consider two possible solutions: (a) $SrRuO_3$, a metallic oxide with a perovskite structure that matches $PbTiO_3$, and (b) Rb, an alkali metal with relatively low cohesive energy.

We first considered adding a single layer of RuO_2 to a PbO-terminated surface, but this turns out to be unstable with respect to the formation of bulk RuO_2. However, adding a full layer of $SrRuO_3$ to a TiO_2-terminated substrate, with the RuO_2 layer on the surface, is stable for all three polarizations. Unfortunately, this surface does not have particularly interesting CO_2 binding properties, as the binding energy is relatively weak and varies

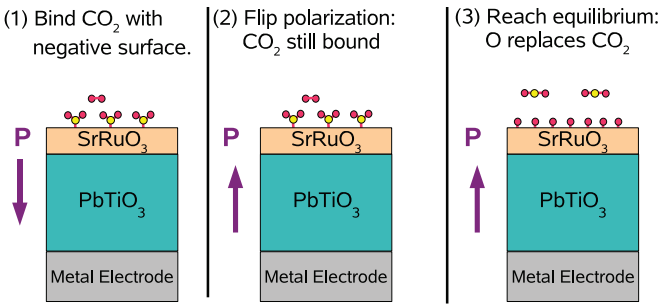

FIG. 16. (Color online) Possible method for reversibly binding CO_2 to a $SrRuO_3$ or SrO monolayer on $PbTiO_3$. Step 1: the CO_2 is bound to the negatively poled surface, which is stable at low O_2 pressure. Step 2: flip the polarization. The CO_2 has a similar binding energy for either polarization; however, the positively poled stoichiometric surface is not thermodynamically stable for experimentally realizable oxygen chemical potentials. Step 3: the system reaches thermodynamic equilibrium, and oxygen replaces the CO_2. To get back to the initial configuration, one flips the polarization back.

only 0.1 eV between positive and negative polarization [see Table V and Fig. 17(a)]. However, the change in oxygen binding is much larger, on the order of 1 eV (see Table V), and it is likely the positively poled surface will be covered in excess oxygen, eliminating all CO_2 binding sites. This suggests that it would be possible to bind CO_2 with the negatively poled surface, and then release it by flipping the polarization, causing oxygen to replace the CO_2 (see Fig. 16).

We also consider adding a single layer of SrO to a TiO_2-terminated $PbTiO_3$ substrate, without a RuO_2 layer. This configuration is thermodynamically stable with respect to SrO formation, and promisingly, CO_2 binds strongly to this surface. All three polarizations bind in the $(CO_3)^{2-}$ geometry and have a binding energy above 1.3 eV [see Table V and Fig. 17(b)]. However, the binding of O to this surface is very strong, especially for the positively poled surface (see Table V), and it is again likely the positively poled surface will be covered in oxygen. Therefore this surface is also a candidate for the cycle proposed in Fig. 16.

Finally, we tried adding 0.5-ML Rb to the $PbTiO_3$ surface, in a $c(2 \times 2)$ configuration. The Rb was stable with respect to the formation of bulk Rb on both stoichiometric terminations of the $PbTiO_3$ surface for all three polarizations; however, the positively poled surface strongly prefers to oxidize and form a layer of rubidium oxide on the surface. We focus our attention on the TiO_2-terminated negatively poled and paraelectric surfaces with 0.5-ML Rb, which our calculations predict could be stabilized under realistic conditions. We find that the addition of Rb increases the binding of CO_2 to these surfaces [see Fig. 17(c)]. While both polarizations bind the CO_2 in a $(CO_3)^{2-}$ geometry regardless of the presence of the Rb, the extra interaction with the Rb increases the binding of CO_2 by 0.2 eV for the negatively poled surface and 1.4 eV on the paraelectric surface, making Rb an interesting candidate for increased CO_2 binding (see Table V as compared with Table I).

VI. CONCLUSIONS

We have examined the effects of polarization on the electronic structure, stoichiometry, geometry, and reactivity of the $PbTiO_3$ surface. We find that polarization has the largest effect on the stoichiometric TiO_2-terminated surface. This surface displays an electronic reconstruction, with electrons or

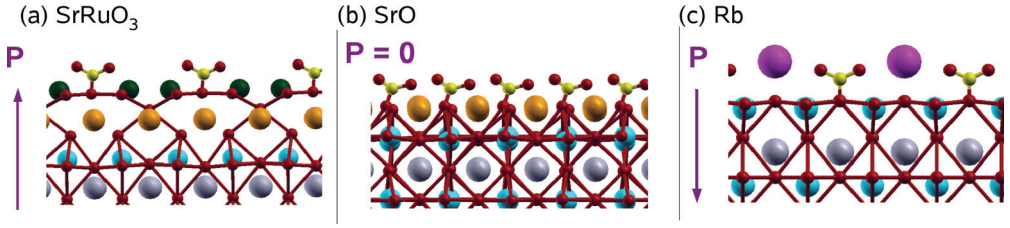

FIG. 17. (Color online) Binding of 0.5 ML CO_2 to selected surfaces. Ru is in dark green, Sr is in orange, Rb is in pink (other colors the same as Fig. 1). (a) Positively poled $SrRuO_3$ surface. (b) Paraelectric SrO surface. (c) Negatively poled surface with 0.5-ML Rb.

holes moving to compensate the polarization-induced surface charge. These electrons and holes have a large effect on CO_2 binding geometry and energy.

Polarization also greatly affects the thermodynamic stability of various surface stoichiometries and geometries. The surface always prefers to screen the depolarization field with atomic reconstructions rather than electronic reconstructions. These atomic reconstructions also affect both CO_2 and H_2O binding by changing both the binding energy and the availability of binding sites.

These results also have a variety of potential applications. If the stoichiometric TiO_2-terminated surface can be stabilized, the positively poled surface would be very interesting substrate for CO_2 catalysis. More realistically, the thermodynamically stable PbO-terminated surfaces also display differences in binding energies of CO_2 and H_2O. However, more work must be done to increase the magnitude of binding for CO_2 and to learn how to take advantage of the dissociation of H_2O when the surface becomes polarized. Finally, by engineering the $PbTiO_3$ by adding monolayers of other oxides to the surface, it is possible to both increase the binding of CO_2 to the surface and also achieve differences in binding with polarization. In particular, the variation of oxygen coverage with polarization provides a method for controlling the availability of CO_2 binding sites.

ACKNOWLEDGMENTS

We wish to acknowledge many helpful discussions with Eric Altman. This work has been supported primarily by the National Science Foundation under MRSEC DMR 0520495 and MRSEC DMR 1119826, in part by the facilities and staff of the Yale University Faculty of Arts and Sciences High Performance Computing Center and by the National Science Foundation under grant number CNS 0821132 that partially funded acquisition of the facilities, and in part by the National Science Foundation through TeraGrid computational resources provided by grant number TG-MCA08X007.

*kgarrity@physics.rutgers.edu

[1] K. F. Garrity, A. M. Kolpak, S. Ismail-Beigi, and E. I. Altman, Adv. Mater. **22**, 2969 (2010).
[2] A. M. Kolpak, I. Grinberg, and A. M. Rappe, Phys. Rev. Lett. **98**, 166101 (2007).
[3] T. Bligaard, J. Nrskov, S. Dahl, J. Matthiesen, C. Christensen, and J. Sehested, J. Catal. **224**, 206 (2004).
[4] S. Dahl, A. Logadottir, C. J. H. Jacobsen, and J. K. Nrskov, Appl. Catal., A **222**, 19 (2001).
[5] Y. Yun and E. I. Altman, J. Am. Chem. Soc. **129**, 15684 (2007).
[6] Y. Yun, L. Kampschulte, M. Li, D. Liao, and E. I. Altman, J. Phys. Chem. C **111**, 13951 (2007).
[7] J. Garra, J. M. Vohs, and D. A. Bonnell, Surf. Sci. **603**, 1106 (2009).
[8] D. Li, M. H. Zhao, J. Garra, A. M. Kolpak, A. M. Rappe, D. A. Bonnell, and J. M. Vohs, Nat. Mat. **7**, 473 (2008).
[9] M. H. Zhao, D. A. Bonnell, and J. M. Vohs, Surf. Sci. **602**, 2849 (2008).
[10] M. H. Zhao, D. A. Bonnell, and J. M. Vohs, Surf. Sci. **603**, 284 (2009).
[11] R. V. Wang, D. D. Fong, F. Jiang, M. J. Highland, P. H. Fuoss, C. Thompson, A. M. Kolpak, J. A. Eastman, S. K. Streiffer, A. M. Rappe *et al.*, Phys. Rev. Lett. **102**, 047601 (2009).
[12] C. Park and R. T. K. Baker, Chem. Mater. **14**, 273 (2002).
[13] C. Park and R. T. K. Baker, J. Phys. Chem. B **104**, 4418 (2000).
[14] Y. Inoue and Y. Watanabe, Catal. Today **16**, 487 (1993).
[15] N. Saito, Y. Yukawa, and Y. Inoue, J. Phys. Chem. B **106**, 10179 (2002).
[16] *IPCC, Climate Change 2007: The Physical Science Basis*, edited by S. Solomon, D. Oin, M. Manning, Z. Chen, M. Marquis, K. B. Averyt, M. Tignor, and H. L. Miller (Cambridge University Press, Cambridge, UK, 2007).
[17] B. Metz, O. Davidson, H. de Coninck, M. Loos, and L. Meyer, *IPCC Special Report: Carbon Dioxide Capture and Storage* (Cambridge University Press, Cambridge, UK, 2005).
[18] D. Oxtoby, H. P. Gillis, and A. Campion, *Principles of Modern Chemistry*, 5th ed. (Brooks Cole, Pacific Grove, CA, 2002).
[19] P. Hohenberg and W. Kohn, Phys. Rev. **136**, B864 (1964).
[20] W. Kohn and L. Sham, Phys. Rev. **140**, A1133 (1965).
[21] J. P. Perdew, J. A. Chevary, S. H. Vosko, K. A. Jackson, M. R. Pederson, D. J. Singh, and C. Fiolhais, Phys. Rev. B **48**, 4978 (1993).
[22] D. Vanderbilt, Phys. Rev. B **41**, 7892 (1990).
[23] For Pb, we include $5d$, $6s$, and $6p$ projectors with cutoff radii $r_d = 2.3$ and $r_s = r_p = 2.3$ Bohr. For Ti, we include semicore $3s$ and $3p$ projectors as well as $3d$, $4s$, and $4p$. Cutoff radii are $r_s = r_p = 1.8$ Bohr and $r_d = 2.0$ Bohr. For O, we include $2s$ and $2p$ projectors with $r_s = r_p = 1.3$ Bohr. For H, we include a $1s$ projector with $r_s = 0.9$ Bohr. For Sr, we include $4s$ and $4p$ semicore states, as well as $4d$, $5s$, and $5d$ states with $r_s = 1.3$ Bohr and $r_p = r_d = 2.2$ Bohr. For Ru, we include $4d$, $5s$, and $5p$ projectors with $r_d = 2.0$ Bohr and $r_s = r_p = 2.2$ Bohr. For Rb, we include $4s$ and $4p$ semicore states plus $4d$, $5s$, and $5p$ projectors with $r_s = 1.8$ Bohr, $r_p = 2.0$ Bohr, and $r_d = 2.2$ Bohr. For Ba, we include $5s$ and $5p$ semicore states

in addition to $5d$, $6s$, and $6p$ projectors, with $r_s = 2.4$ Bohr, $r_p = 2.0$ Bohr, and $r_d = 2.2$ Bohr.
[24]L. Bengtsson, Phys. Rev. B **59**, 12301 (1999).
[25]S. Venkatesan, A. Vlooswijk, B. J. Kooi, A. Morelli, G. Palasantzas, J. T. M. DeHosson, and B. Noheda, Phys. Rev. B **78**, 104112 (2008).
[26]H. J. Freund and M. W. Roberts, Surf. Sci. Rep. **25**, 225 (1996).
[27]S. V. Levchenko and A. M. Rappe, Phys. Rev. Lett. **100**, 256101 (2008).
[28]K. Reuter and M. Scheffler, Phys. Rev. B **65**, 035406 (2001).
[29]K. F. Garrity and S. Ismail-Beigi, Phys. Rev. B **80**, 085306 (2009).
[30]*NIST Chemistry WebBook* (2010), http://webbook.nist.gov/chemistry/.
[31]M. M. Lenkcka and R. E. Riman, Chem. Mater. **5**, 61 (1993).
[32]Y. Zhang and W. Yang, Phys. Rev. Lett. **80**, 890 (1998).
[33]E. J. Walter and A. M. Rappe, Surf. Sci. **427-428**, 11 (1999).
[34]B. Hammer, L. B. Hansen, and J. K. Norskov, Phys. Rev. B **59**, 7413 (1999).
[35]A. M. Kolpak and S. Ismail-Beigi, Phys. Rev. B **83**, 165318 (2011).
[36]B. Meyer, J. Padilla, and D. Vanderbilt, Faraday Discuss. **114**, 395 (1999).
[37]A. Munkholm, S. K. Streiffer, M. V. Ramana Murty, J. A. Eastman, C. Thompson, O. Auciello, L. Thompson, J. F. Moore, and G. B. Stephenson, Phys. Rev. Lett. **88**, 016101 (2001).
[38]P. A. Redhead, Vacuum **12**, 203 (1962).